Environ Monit Assess (2020) 192:269
https://doi.org/10.1007/s10661-020-8216-3

Integrating drone imagery with existing rangeland monitoring programs

Jeffrey K. Gillan · Jason W. Karl · Willem J. D. van Leeuwen

Received: 13 November 2019 / Accepted: 16 March 2020

Abstract The recent availability of small and low-cost sensor carrying unmanned aerial systems (UAS, commonly known as drones) coupled with advances in image processing software (i.e., structure from motion photogrammetry) has made drone-collected imagery a potentially valuable tool for rangeland inventory and monitoring. Drone-imagery methods can observe larger extents to estimate indicators at landscape scales with higher confidence than traditional field sampling. They also have the potential to replace field methods in some instances and enable the development of indicators not measurable from the ground. Much research has already demonstrated that several quantitative rangeland indicators can be estimated from high-resolution imagery. Developing a suite of monitoring methods that are useful for supporting management decisions (e.g., repeatable, cost-effective, and validated against field methods) will require additional exploration to develop best practices for image acquisition and analytical workflows that can efficiently estimate multiple indicators. We embedded with a Bureau of Land Management (BLM) field monitoring crew in Northern California, USA to compare field-measured and imagery-derived indicator values and to evaluate the logistics of using small UAS within the framework of an existing monitoring program. The unified workflow we developed to measure fractional cover, canopy gaps, and vegetation height was specific for the sagebrush steppe, an ecosystem that is common in other BLM managed lands. The correspondence between imagery and field methods yielded encouraging agreement while revealing systematic differences between the methods. Workflow best practices for producing repeatable rangeland indicators is likely to vary by vegetation composition and phenology. An online space dedicated to sharing imagery-based workflows could spur collaboration among researchers and quicken the pace of integrating drone-imagery data within adaptive management of rangelands. Though drone-imagery methods are not likely to replace most field methods in large monitoring programs, they could be a valuable enhancement for pressing local management needs.

Keywords Drone · Unmanned aerial system · Rangelands · Adaptive management · Ecological inventory and monitoring · Remote sensing

Electronic supplementary material The online version of this article (https://doi.org/10.1007/s10661-020-8216-3) contains supplementary material, which is available to authorized users.

J. K. Gillan (✉) · W. J. van Leeuwen
School of Natural Resources and the Environment, University of Arizona, Tucson, AZ 85721, USA
e-mail: jgillan@email.arizona.edu

W. J. van Leeuwen
e-mail: leeuw@email.arizona.edu

J. W. Karl
Department of Forest, Rangeland, and Fire Sciences, University of Idaho, Moscow, ID 83844, USA
e-mail: jkarl@uidaho.edu

W. J. van Leeuwen
School of Geography and Development, University of Arizona, Tucson, AZ 85721, USA

Published online: 06 April 2020

Introduction

Rangeland inventory and monitoring (I & M) data, used to evaluate ecosystem function and successional states, are important for adaptive management of public and private rangelands (Allen et al. 2017; Kendall and Moore 2012; Mitchell 2010). The Bureau of Land Management's (BLM) assessment, inventory, and monitoring (AIM) strategy is an I & M program intended to provide long-term data on the status and trend of land health (biotic integrity, soil and site stability, hydrologic function) across all BLM managed lands in the American West (Taylor et al. 2014; Toevs et al. 2011). AIM uses standardized field-data collection methods, and randomized (i.e., probability-based) sampling designs to infer the status and trend of rangeland health indicators across reporting areas that could include grazing allotments, watersheds, or entire field offices. However, in landscape units with heterogeneous or patchy vegetation characteristics, a field sampling approach that observes only a small fraction of the inference area (as many field-based monitoring programs do) may estimate indicator values and their change with low confidence (Booth and Cox 2011).

The recent availability of small and low-cost sensor carrying unmanned aerial systems (UAS, commonly known as drones) along with the codification of piloting and airspace rules has made drone-collected imagery a potentially valuable tool for range inventory and monitoring. Small drones (< 5 kg) can now be easily brought into the field and deployed to image dozens to hundreds of hectares at spatial resolutions capable of measuring fine-scale vegetation and soil indicators. They hold the promise of observing larger extents and estimating I & M indicators at landscape scales with higher confidence than traditional field sampling. Drone imagery methods also have the potential to replace field methods in some instances (Cunliffe et al. 2016; Gillan et al. 2017; Olsoy et al. 2018), and enable the development of indicators not measurable from the ground (Ludwig et al. 2007; Rango et al. 2009).

Research has shown that several quantitative rangeland indicators can be estimated from high-resolution imagery (< 10 cm ground sampling distance (GSD)). Fractional cover estimates have been demonstrated using classification algorithms (Baena et al. 2017; Cruzan et al. 2016; Laliberte et al. 2010a, b, 2011a, b; Laliberte and Rango 2011; Lu and He 2017; McGwire et al. 2013) and visual interpretation (Booth and Cox 2008, 2009; Breckenridge et al. 2011; Duniway et al. 2012; Hardin et al. 2007; Karl et al. 2014; Moffet 2009; Seefeldt and Booth 2006) with high success for plant functional types and some species identification. From high-resolution imagery, it is possible to estimate large inter-canopy gaps (Karl et al. 2012; Rango et al. 2009) as well as vegetation heights and structure (Cunliffe et al. 2016; Gillan et al. 2014; Jensen and Mathews 2016; Olsoy et al. 2018; Swetnam et al. 2018).

However, for drone-based methods to gain widespread use for I & M, including integration with existing programs, they need to be repeatable, cost-effective, and validated against current field methods. Because best practices for estimating a suite of I & M indicators will vary by vegetation composition and phenology, it seems unlikely and perhaps unproductive to pursue a standard set of protocols as have been developed for field methods (e.g., AIM core indicators; MacKinnon et al. 2011). Instead, image acquisition and analytic workflows will need to be customized by ecosystem including timing of data collection conducive to detecting the I & M features of interest (Hunt et al. 2003; Lass and Calihan 1997). For the sake of efficiency, workflows should be designed to estimate multiple indicators when possible.

In this paper, we present the results of a pilot program to test the use of image products collected from small UAS to produce multi-indicator rangeland I & M data. For this test, we embedded with a BLM field monitoring crew in Northern California, USA to compare field-measured and imagery-derived indicator values and to evaluate the logistics of using small UAS as a field-deployed tool for rangeland monitoring. We sought to develop image acquisition and processing methods specific for the sagebrush steppe, an ecosystem that is common in other BLM managed lands. Accordingly, the methods described in this paper could be applied to other similar vegetation communities.

Our objectives were to (1) develop a unified workflow to measure three common rangeland indicators from drone imagery: fractional cover of plant functional types, canopy gaps, and vegetation heights; (2) assess agreement between imagery-based indicator values and field-measured values; and (3) investigate how fractional cover estimates differed between two different sensor types.

Material and methods

Study area

Field research was conducted at the Applegate and Eagle Lake field offices in the BLM's Northern California District (NCD), in northeastern California, and across the border into Nevada (Fig. 1). The combined land area of both field offices is 11,165 km^2 and consists primarily of semi-arid sagebrush steppe, scattered mountain ranges reaching elevation of 2500 m, and extensive desert playas devoid of vegetation. Mean annual precipitation ranges from 25 to 35 cm with 75% occurring between October and March. Typically, the warmest month is July with average temperature highs of 31.5 °C and lows of 10.4 °C. January is typically the coldest month of the year with average temperature highs of 4.7 °C and lows of − 6 °C. A primary use of BLM lands in the NCD is cattle grazing. Greater sage-grouse (*Centrocercus urophasianus*), a species of conservation concern, has critical habitat within the district (US Bureau of Land Management 2007). The district has been heavily invaded by cheatgrass (*Bromus tectorum*) which has led to large range fires such as the Rush Fire in 2012. There are also large populations of wild horses and burros.

Field data collection

Three-person crews collected field data following the protocols of the BLM's AIM strategy (Herrick et al. 2017). A total of 122 plots were visited and sampled in the NCD between May 22 and September 11, 2017. At each plot, three 25-m transects were established radiating out from the plot's center to form a "spoke" plot design, oriented at magnetic 0°, 120°, and 240°, respectively (Fig. 2). The transects started 5 m away from the plot center where equipment was stored and a soil pit dug to determine soil type and ecological site.

Along each transect, fractional cover was estimated using the line-point intercept method (Herrick et al. 2017). Every 0.5 m along the transect, an observer dropped a 1-mm-diameter metal pin to the ground without directing its landing location. Vegetation intercepted by the pin was recorded to species. The "top-hit" (i.e., foliar cover) was recorded along with any lower vegetation touched by the pin. Ground surface was recorded for each pin drop as bare soil, rock, litter, or biological crust regardless of whether vegetation was also encountered. Each transect had 50 observations, and transects were aggregated to form a plot sampling unit with a total of 150 observations. To facilitate comparison with imagery fractional cover, we used just the "top-hit" vegetation to calculate cover. Cover (as a proportion) was calculated by dividing the number of observations of a given cover class by the total number of observations.

Vegetation heights were measured along the same transects at 2.5-m intervals (30 total measurements per plot). The height and species of the tallest herbaceous and woody vegetation, encountered within a 15-cm radius of a rod, was recorded to the nearest cm (Herrick et al. 2017). This included any dead or dormant plant. For the purposes of this study, only woody vegetation heights were compared with drone imagery.

Inter-canopy gaps were measured along the three transects following Herrick et al. (2017). Field crews recorded the distances (in cm) between vegetation canopies (woody or herbaceous) with only gaps > 25 cm being recorded. The canopy gap indicator was reported as the percentage of the total transect length for gap sizes of 25–50 cm, 51–100 cm, 101–200 cm, and > 200 cm as recommended by Herrick et al. (2017).

Developing a unified workflow for multiple indicators

Designing the acquisition and image processing workflow tailored to the NCD study area began with an extensive literature review of previous studies using very high-resolution imagery to estimate fractional cover and vegetation heights (Fig. 3). While these studies present varied methods, collectively, they represent the myriad choices for turning very high-resolution imagery into quantitative estimates of ecosystem indicators. Breaking down each paper's workflow into its component parts helped to reveal the popularity of choices for each decision and identify gaps in research (i.e., viable choices that have not been tested). In addition, we documented (in graphical form) the step-by-step instructions to produce each of the indicators (Fig. 4).

UAS image acquisition

We acquired UAS imagery at 16 AIM plots in NCD between June 16 and July 1, 2017 (Fig. 1; supplemental Table A1). At 12 of the plots, we collected the imagery 2–5 days after the field crews had collected their data. For the remaining four plots, we embedded with the

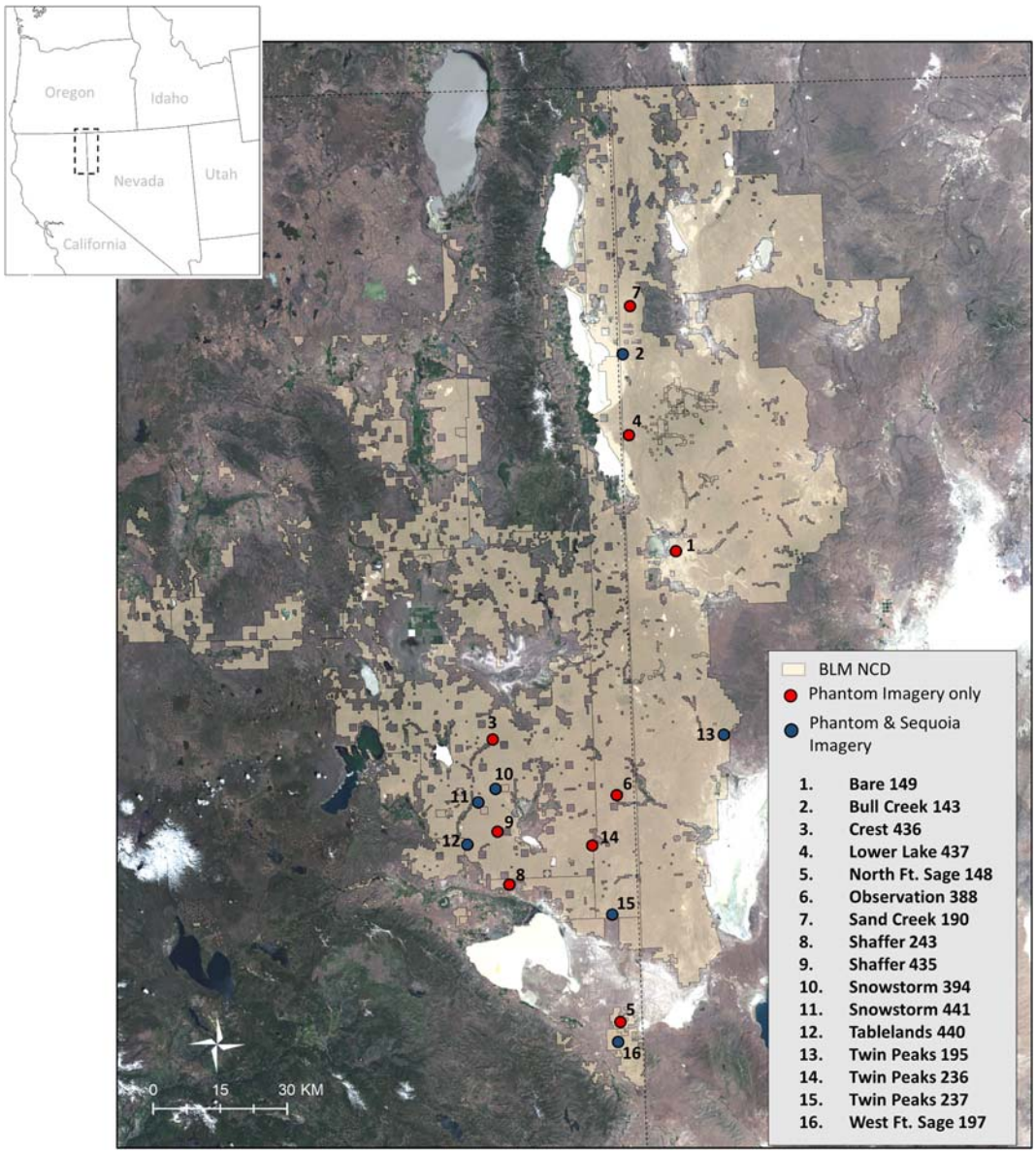

Fig. 1 Study area at the Northern California District (NCD) of the Bureau of Land Management. BLM land is highlighted in tan. Red circles indicate AIM plot locations where only Phantom imagery was collected, while blue circles are plot locations where Phantom and Sequoia imagery were acquired. The background imagery is from Landsat 8, acquired June 2017

field crew and acquired the imagery immediately before the field measurements. Accessing all of the plot locations required off-trail hiking across rugged terrain with the drones and associated equipment carried in backpacks. We chose the plots to cover a range of ecological sites and vegetation communities in coordination with the field crew's monitoring schedule. Drones were operated under a Part 107 small UAS license with a special use permit to conduct air operations over BLM land.

We acquired aerial imagery with Phantom 3 Professional and Phantom 4 quad-rotor drones (https://www.dji.com). Both drones have nearly identical 12-megapixel integrated RGB sensors (Table 1). We also employed a Parrot Sequoia sensor (https://www.parrot.com), which we mounted on the Phantom 3. The Sequoia is a very small multi-spectral sensor with green, red, red-edge, and near-infrared (NIR) bands (Table 1). With its own external power supply, global navigation

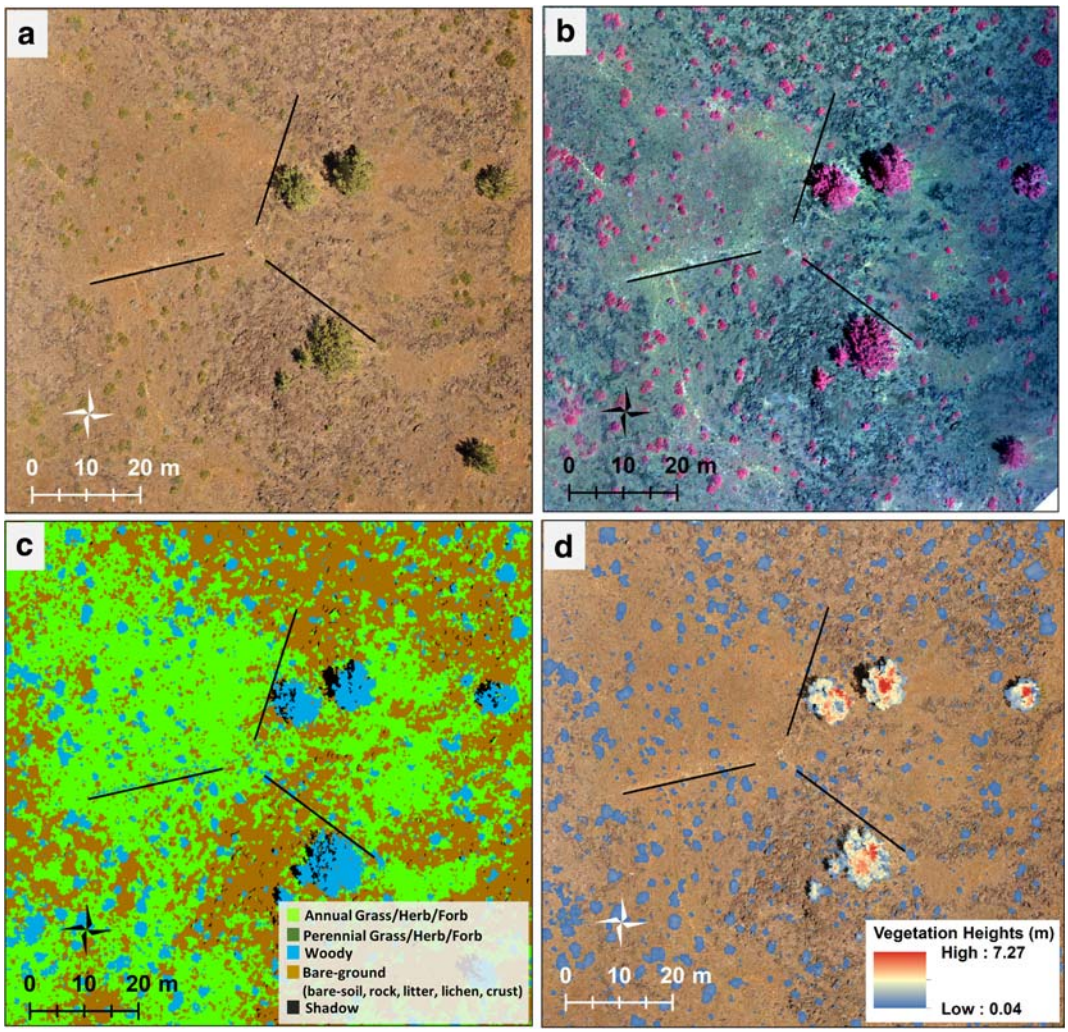

Fig. 2 Data for this study were collected at field plots consisting of three 25-m transects (black lines). Shown here is plot Tablelands 440. **a** Orthomosaic made with Phantom RGB imagery. **b** False-color composite orthomosaic made with Sequoia multi-spectral imagery. **c** An orthomosaic thematically classified into plant functional types, **d** Woody vegetation heights

satellite system, and sensor-triggering capabilities, the Sequoia operated independently from the drone.

Autonomous grid pattern missions were programmed in Altizure v 3.0 (https://next.altizure.com). We flew one mission to collect nadir (vertical) imagery and four missions to collect 30° oblique images because prior research has shown that the incorporation of oblique images into photogrammetry can improve scene geometry (James and Robson 2014). We collected imagery 40 m above ground level (AGL) at each plot, yielding GSD of 1.5 cm for the Phantom imagery and 3.7 cm for the Sequoia imagery (Table 1). This resolution was chosen because it was determined to be fine enough to detect the presence of bunch grasses while limiting excessive processing time typical of finer-scale data (see Gillan et al. 2019). Sequoia imagery was collected on only seven plots due to a manufacturer defect that caused the sensor to overheat (see Fig. 1 for plot locations and Table A1 for plot details). At each plot, we collected between 210 and 280 images per sensor covering an area slightly larger than the AIM plot (~ 1 ha). Radiometric calibration of the drone-collected images was deemed unnecessary because all classification, analysis, and interpretation was conducted within individual plots using images that were collected during a single drone flight.

Though the Phantom drones and Sequoia sensor record geographic coordinates of each acquired image

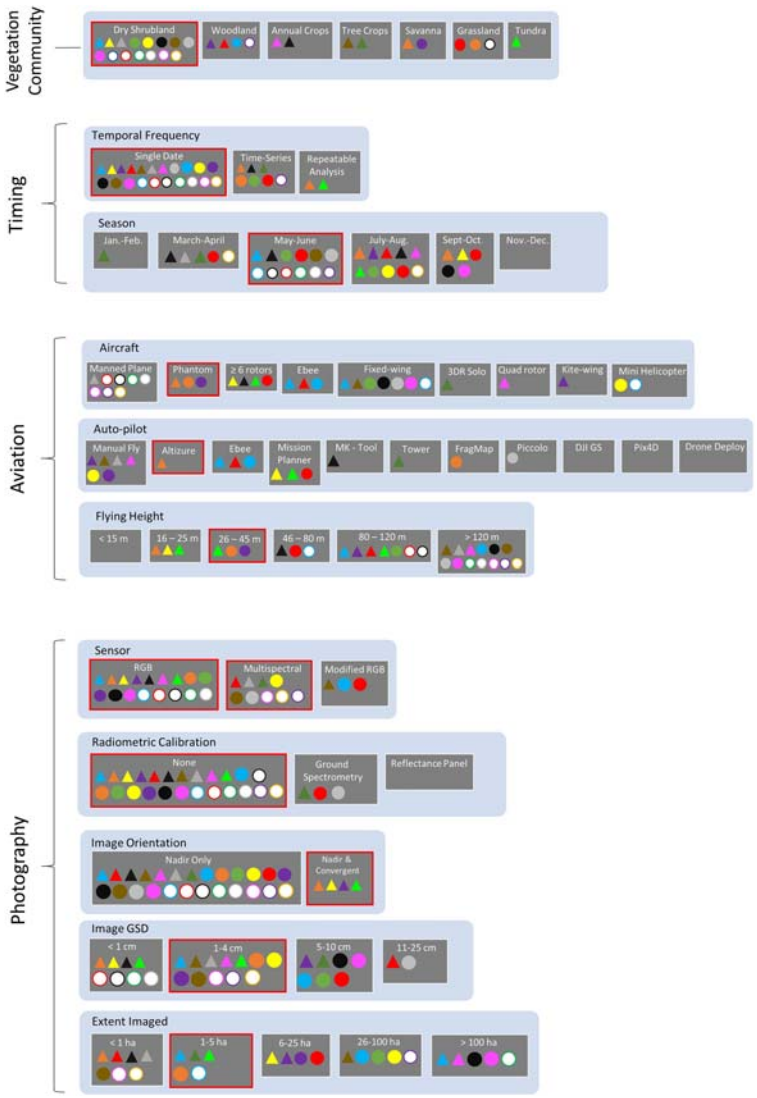

Fig. 3 Workflow decisions based on a review of 29 published studies using high-resolution aerial photography (drone and manned aircraft) to estimate vegetation fractional cover and height. The focus was on rangeland type environments (e.g., grasslands, shrublands) but also included some research in crop systems. The options used in this project are highlighted with red boxes

with their onboard global navigation satellite systems (GNSS), they are typically accurate to only a few meters horizontally, and several meters vertically. Because we visited these remote plots only one time, it was not practical to install and survey ground control points (GCPs) to reference the scenes. To overcome this limitation, we placed a single 8-m long scale-bar in the center of each plot instead of surveying GCPs (sensu Carbonneau and Dietrich 2016). The scale-bar consisted of two aerial targets on the ends of an 8-m collapsible rod. Informing the photogrammetry software of an object of known length (i.e., scale-bar) ensures correct horizontal and vertical dimensions for the entire image model, enabling accurate estimates of fractional cover and vegetation heights (Carbonneau and Dietrich 2016). At a test plot in southern New Mexico, we found scale-bar reference point clouds to be within 2 cm horizontally and 2.5 cm vertically of point clouds using a network of surveyed ground control points. Using this approach, however, the image products may be systematically shifted both horizontally and vertically compared to their true location (i.e., georeferencing error).

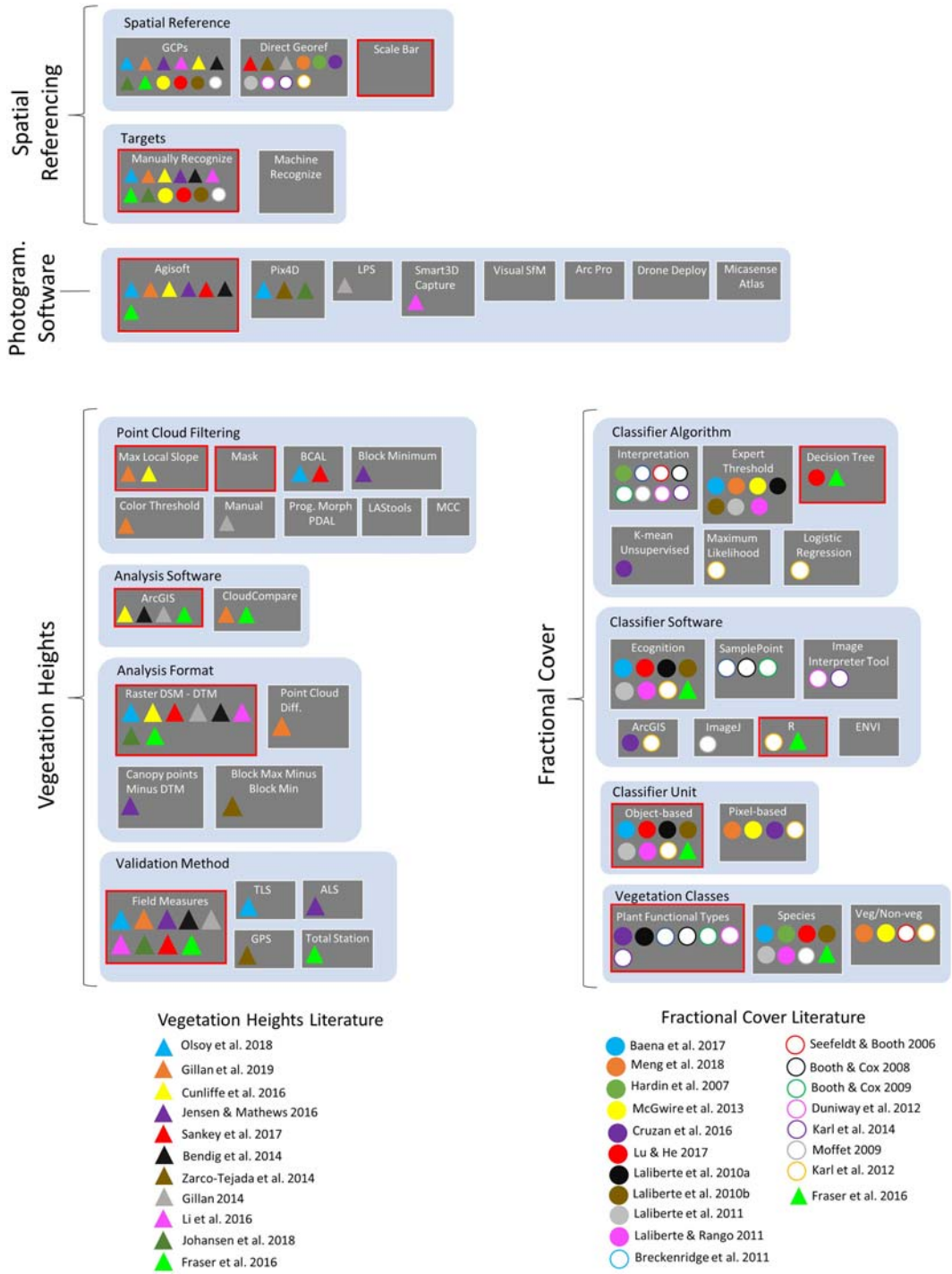

Fig. 3 (continued)

Photogrammetry and image product creation

We used structure-from-motion photogrammetry (SfM) software Agisoft Photoscan v. 1.3.5 (www.agisoft.com) to make point clouds and orthomosaics of each plot and sensor separately. The general SfM process of making point clouds is well-documented (Eltner et al. 2015; Smith et al. 2015; Snavely et al. 2008; Westoby et al.

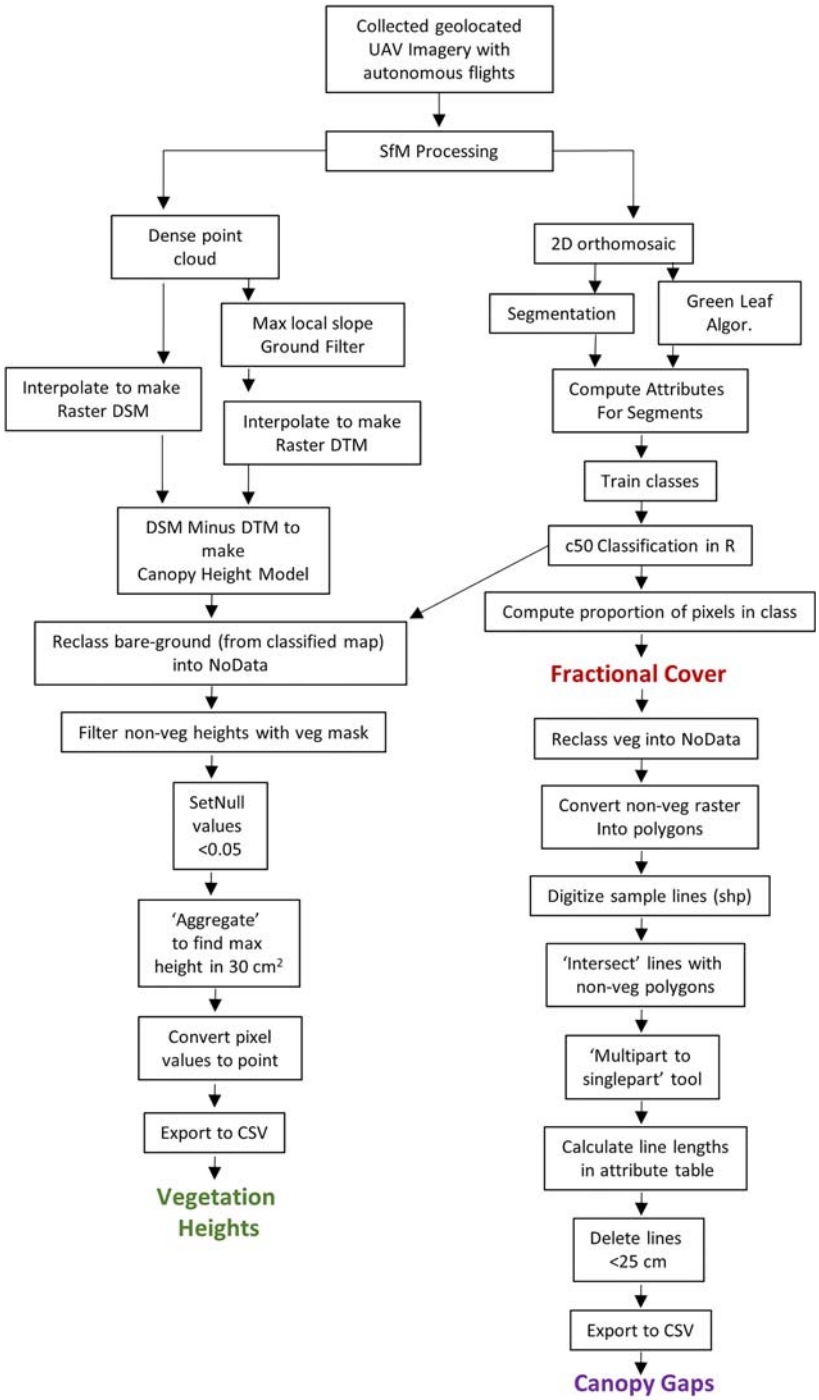

Fig. 4 Step-by-step workflow to calculate vegetation fractional cover by plant functional types, canopy gaps, and vegetation heights from orthomosaics and point clouds

2012), so it will be abbreviated here. All image processing was carried out on a Windows 10 machine with two Intel Xeon CPUs (2.4 GHz; 16 logical processors each), two EVGA GeForce GTX 1080 video cards, and 256 GB RAM. We did "high quality" initial alignment and self-calibration using the latitude, longitude, and

Table 1 Phantom 3 and 4 camera and Parrot Sequoia sensor specifications

	Spectral characteristics	Sensor pixels	Shutter	Radiometric resolution	Image format	Image overlap	GSD at 40 m AGL
Phantom 3 and 4	Red, green, blue	4000 horizontal × 3000 vertical (12 mpx)	Rolling with 33 ms readout	8 bit (256 BVs)	jpeg	75–80%	1.5 cm
Parrot Sequoia	Green 530–570 nm Red 640–680 nm Red-edge 730–740 nm NIR 770–810 nm	1280 horizontal × 960 vertical (1.2 mpx)	Global	10 bit (1024 BVs) stored as 16 bit (65,536 BVs)	Tiff	75–80%	3.7 cm

elevation stamped on each image. To improve model scaling, we referenced each plot with a single 8-m scale-bar (see Carbonneau and Dietrich 2016). We estimated the scale-bar length accuracy to be within 5 cm. Following the recommendation of James et al. (2017), we optimized parameters focal length (f), principal point coordinates (cx, cy), radial distortion (k1, k2), and tangential distortion (p1, p2), and also for rolling shutter effect present in Phantom sensors (Vautherin 2016). Next, we used the "gradual selection" tool to identify and remove low-quality sparse points with the following criteria: reprojection error > 0.3 pixels, reconstruction uncertainty > 13, and projection error > 10. The sparse cloud was optimized (bundle adjustment) after each removal of low quality points. For dense point cloud reconstruction, we used just the nadir images. Extensive testing found that nadir only dense point clouds were nearly identical to nadir + all oblique images with resolution of 1.5 cm. Using only nadir images greatly reduced the processing time from multiple days to a few hours per plot. Point clouds were generated at "ultra high" density which attempted to generate a point at every pixel. Point cloud densities were typically 1000–3000 points·m^{-2}.

Orthomosaic generation required a slightly different workflow. Experience has shown that very detailed point clouds and subsequent digital elevation models (DEMs) create orthomosaics with substantial stretching and artifacts. Accordingly, we generated a dense point clouds with low density followed by the creation of low-resolution DEMs (6–10 cm depending on the scale of the imagery) used in the orthorectification process. Orthomosaic spatial resolutions were 1.5 cm for Phantom imagery (Fig. 2a) and 3.7 cm for Sequoia imagery (Fig. 2b).

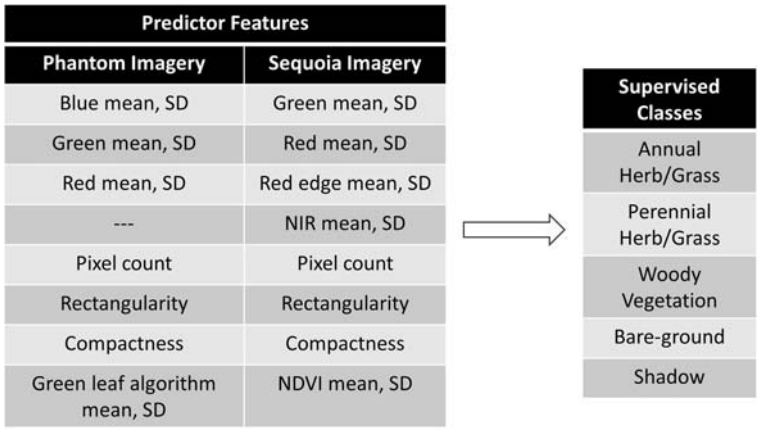

Fig. 5 Image features used to predict supervised classes in c50 decision tree classification

UAS imagery indicator generation

Classifying fractional cover

Prior to orthomosaic classification, we simplified the images through segmentation (i.e., grouping similar contiguous pixel together into objects; Burnett and Blaschke 2003). With very high spatial resolution, classification on segments (or objects) have been shown to be more accurate than pixel-based classifications that suffer from "salt & pepper" heterogeneity within features such as shrub canopies (Laliberte et al. 2011a). Segmentation also facilitates the use of non-color traits such as texture, size, and shape to distinguish classes, while pixel-based classifications can generally only use spectra (Navulur 2007). Using the "segment mean shift" tool in ArcMap 10.5 (https://www.esri.com), we attempted to group pixels into real features on the landscape (e.g., one segment for one shrub). This was quite difficult to achieve so most objects such as shrubs or large rocks often contained multiple segments.

The spectral features we used to classify the Phantom imagery were (Fig. 5) blue mean and standard deviation (SD), green mean and SD, red mean and SD, and green leaf algorithm (GLA; $\frac{G\times 2-R-B}{G\times 2+R+B}$; Louhaichi et al. 2001) mean and SD. Additionally, we used the following spatial features for classification of image segments: segment pixel count, rectangularity, and compactness. For rectangularity, values range from 0 to 1, with 1 being a rectangle. Compactness is the degree to which a segment is circular with values ranging from 0 to 1, where 1 is a circle. For Sequoia imagery, we included the red-edge and NIR bands and used normalized difference vegetation index (NDVI) instead of the green leaf algorithm. We calculated feature values for each segment.

Noticeably absent from the list of features is canopy heights which are frequently used in object-based classifications (Baena et al. 2017; Cruzan et al. 2016). In this workflow, canopy height models were created after vegetation classification and thus could not be used as a feature in the classification (details in 'Vegetation Heights' section).

The final classes were annual herb/grass, perennial herb/grass, woody, bare-ground, and shadow in some cases (Fig. 5). The bare-ground class included bare-soil, rock, and lichen. For classification training, we created individual point shapefiles for each class. We placed 50–100 points per class on the segmented orthomosaics where we opportunistically found representative samples. Identifying specific classes was aided by line-point intercept field data and ground photos. At several plots (West Ft. Sage197, Tablelands 440, Shaffer 243, Twin peaks 236, Crest 436, Snowstorm441, and Lower Lake 437), we omitted perennial herb/grass as a class because it either did not occur in the plot or the specimens were too small and indistinguishable to be useful for training.

We used R package c50 (Kuhn and Quinlan 2017) to classify the orthomosaics. The algorithm, which is an R version of SEE5 (www.rulequest.com/see5-info.html), is a machine learning decision tree used to predict discrete classes. We specified adaptive boosting with 20 trials and disabled winnowing. We used 75% of the training samples to train the classifier and withheld 25% for validation (see Fig. A1 complete R code). C50 outputs confusion matrices and information to assess the importance of predictor features (see Table A2 for feature importance and Table A3 for aggregated confusion matrix). We calculated fractional cover as the number of pixels per class as a proportion of total classified pixels (Fig. 2c).

Canopy gaps

From the classified orthomosaics, we calculated canopy gaps following the general methods presented in Karl et al. (2012). First, we digitized the three transects using markers (iron-cross targets) located at the ends as a reference. We retained the bare-ground class and removed annual herb/grass, perennial herb/grass, and woody classes. We then converted the bare-ground raster into vector polygons and used the "intersect" tool in ArcMap to identify the parts of lines crossing the bare-ground polygons. We calculated the length of each line and created histograms for the proportion of total line length having lengths of 25–50 cm, 51–100 cm, 101–200 cm, and > 200 cm.

Vegetation heights

We calculated vegetation heights using only the Phantom RGB imagery point clouds because the coarser Sequoia imagery would produce less detailed 3D reconstructions. Using the "classify ground points" tool in Agisoft, we identified points representing the ground. This is a type of maximum local slope filter

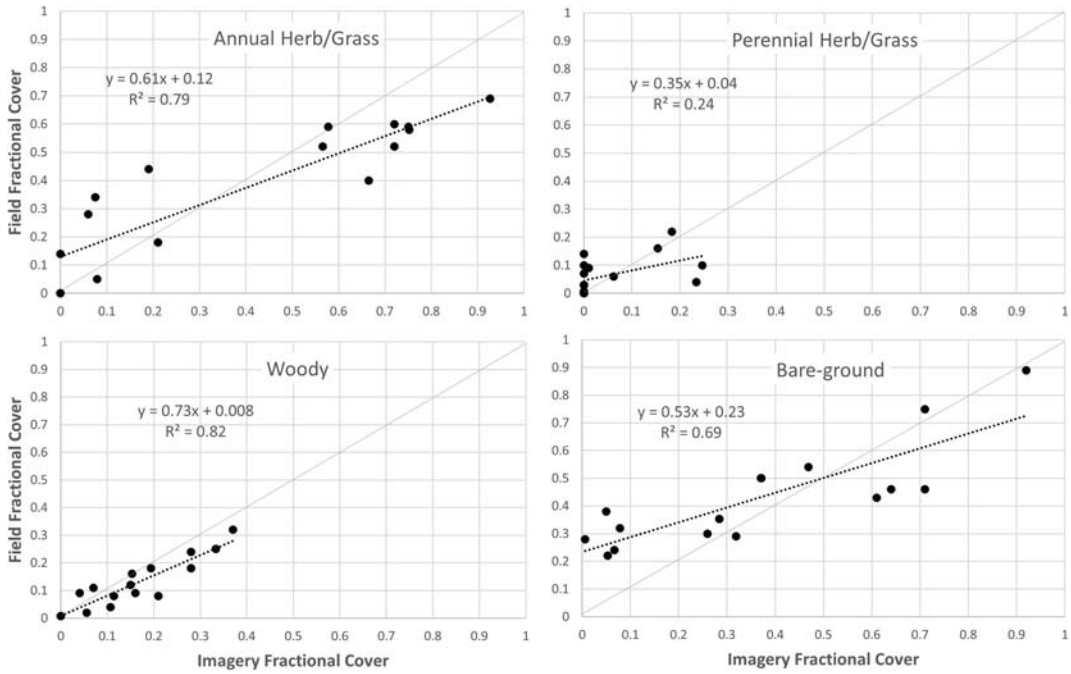

Fig. 6 Scatter plots and linear regression (dotted lines) show the comparison between field and Phantom imagery estimates of fractional cover ($n = 16$). Solid gray lines represent a 1:1 agreement

(Montealegre et al. 2015) where the lowest elevation point within a user defined grid cell is assumed to be the ground. All additional ground points were identified based on a user defined maximum angle and vertical distance from the origin ground point. For each plot, we specified a grid cell size of 2 m with a max angle of 9° and max distance of 10 cm.

In ArcMap, we converted the original point clouds into digital surface models (DSMs) with a 5-cm cell size by assigning the cell value as the highest elevation point and using natural neighbor interpolation to estimate values for cells with no points. Digital terrain models (DTMs) were created similarly with ground-only point clouds. Using "raster calculator," we subtracted the DTM from the DSM on a cell-by-cell basis to create a canopy height model (CHM). In some plots, the presence of large boulders were appearing in the CHMs. To remove the boulders height data, we identified and deleted any height measurements that were not classified as vegetation.

Though this study specifically looked at woody vegetation heights, we chose not to filter herbaceous vegetation out of the CHM. The spatial resolution of the drone imagery was generally too coarse to detect herbaceous vegetation heights (see Gillan et al. 2019), especially for species such as cheatgrass (*Bromus tectorum*) and squirreltail (*Elymus elymoides*) with low-stature growth forms. Analysis of the CHMs showed very little if any registered heights concurrent with the presence of herbaceous vegetation. Finally, we used the "aggregate" tool to compute the highest height value within a 30 × 30 cm grid cell on the CHMs (Fig. 2d) to more closely match the field method of finding the highest part of the plant within a 15-cm radius of the rod.

Table 2 Fractional cover for field data and Phantom RGB imagery. Standard errors are shown in parenthesis

	Data	Annual herb/grass	Perennial herb/grass	Woody	Bare-ground	Shadow
Mean	Field	0.37 (0.05)	0.06 (0.01)	0.12 (0.02)	0.43 (0.04)	0
	Phantom	0.39 (0.08)	0.05 (0.02)	0.15 (0.02)	0.36 (0.07)	0.017
	Difference	0.02 (0.04)	0.00 (0.02)	0.03 (0.01)	− 0.06(0.04)	0.017
Absolute mean	Difference	0.13 (0.02)	0.05 (0.01)	0.04 (0.00)	0.14 (0.02)	0.017

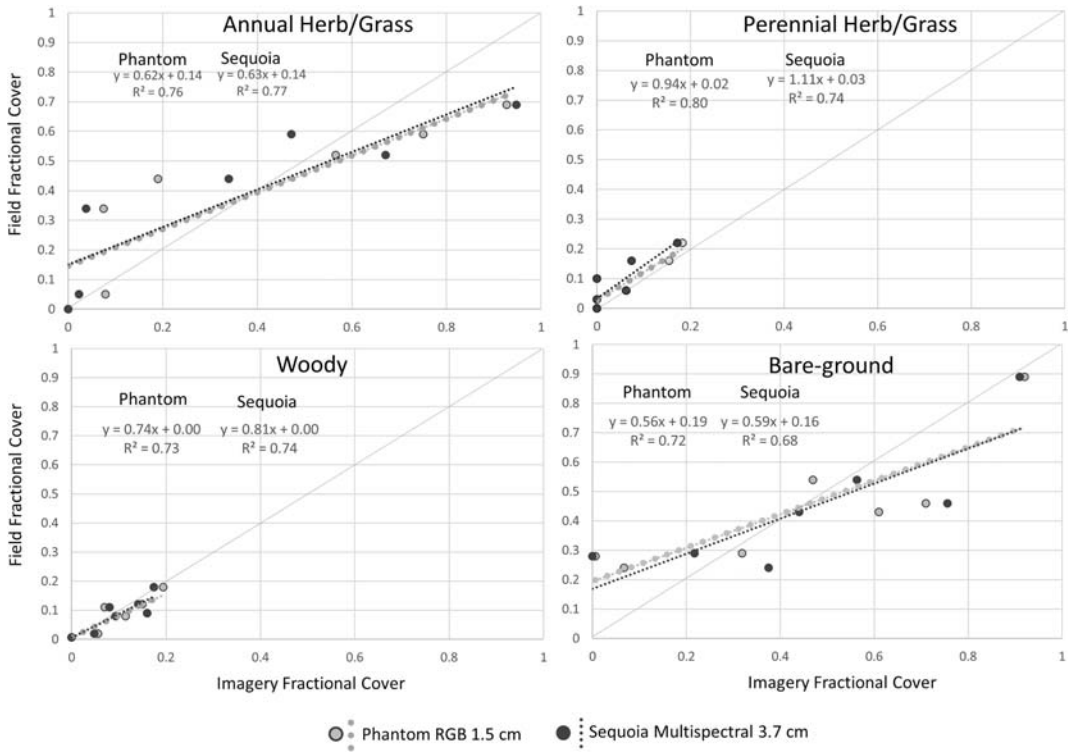

Fig. 7 Fractional cover scatter plots and regression lines showing linear relationships between Phantom RGB imagery and field methods ($n = 7$), and Sequoia multi-spectral imagery and field methods ($n = 7$). Solid lines represent 1:1 agreement

Comparison between field and imagery indicators

We assessed agreement between field and imagery indicator values using the plot as the sample unit. Imagery indicator values for fractional cover and vegetation heights were calculated within rectangular polygons along each field transects' location approximately 0.33 m wide to contain spatial co-registration errors with field measurements. Canopy gap values were estimated along the three transects. For each indicator (fractional cover, canopy gaps, vegetation heights), we assessed method agreement by comparing the mean values (with 95% confidence intervals) across all 16 plots. Mean differences (which include signed differences) were useful for showing bias toward overestimate or underestimate indicator values, while absolute mean differences (which eliminate signed differences) were computed to show true departure between methods.

Table 3 Comparing fractional cover estimated with Phantom RGB and Sequoia multi-spectral imagery ($n = 7$). Standard errors shown in parenthesis

	Data	Annual herb/grass	Perennial herb/grass	Woody	Bare-ground	Shadow
Mean	Field	0.37 (0.09)	0.08 (0.03)	0.08 (0.02)	0.44 (0.08)	0
	Phantom	0.36 (0.14)	0.05 (0.03)	0.10 (0.02)	0.44 (0.12)	0.01
	Sequoia	0.35 (0.13)	0.04 (0.02)	0.09 (0.02)	0.46 (0.11)	0.02
Mean difference with field methods	Phantom	− 0.00 (0.07)	− 0.02 (0.01)	0.01 (0.01)	− 0.00 (0.07)	0.01
	Sequoia	−0.01(0.06)	− 0.03 (0.01)	0.01 (0.01)	0.01 (0.06)	0.02
Absolute mean difference with field methods	Phantom	0.14 (0.04)	0.02 (0.01)	0.03 (0.00)	0.14 (0.03)	0.01
	Sequoia	0.13 (0.04)	0.03 (0.01)	0.02 (0.00)	0.11 (0.04)	0.02

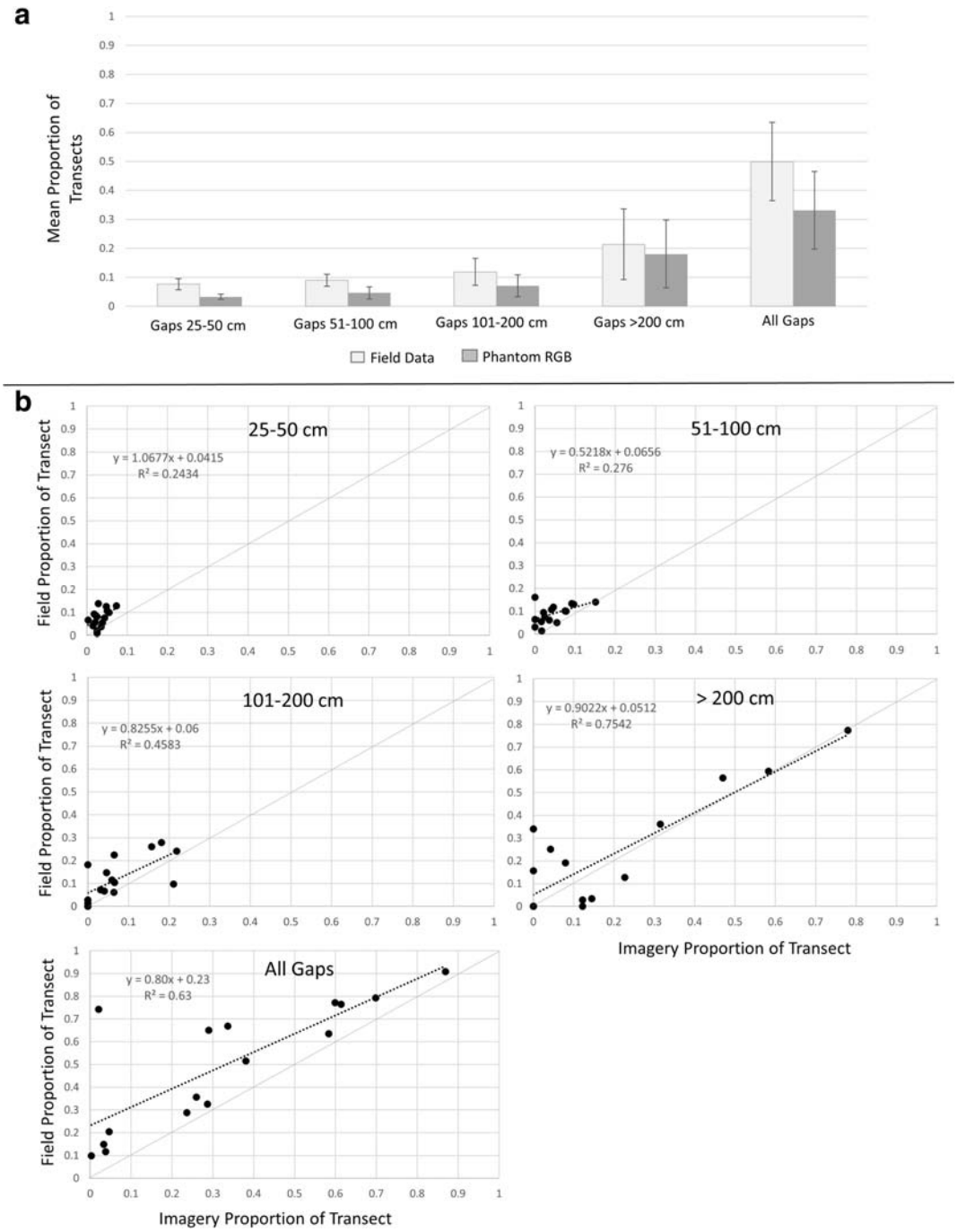

Fig. 8 Canopy gaps comparison between field measurements and imagery. **a** Bars indicate mean proportion of transect with associated gap sizes. Error bars indicate 95% confidence intervals. **b** Scatterplots and linear regression (dotted lines) comparing field and imagery estimates of canopy gaps. Solid lines represent 1:1 agreement

Additionally, we performed least-squares regression and calculated coefficients of determination (R^2 values) to describe linear relationships between methods. For vegetation heights, we additionally compared maximum and standard deviation and the proportion of observations within eight histogram bins. On a subset of plots

Table 4 Comparison of canopy gap data as measured by field and imagery (Phantom) methods

	Data	25–50 cm	51–100 cm	101–200 cm	> 200 cm	All gaps > 25 cm
Mean	Field	0.07 (0.00)	0.09 (0.01)	0.11 (0.02)	0.21 (0.06)	0.49 (0.06)
	Phantom	0.03 (0.00)	0.04 (0.01)	0.071 (0.01)	0.18 (0.05)	0.33 (0.06)
	Difference	− 0.04 (0.00)	− 0.04 (0.01)	− 0.04 (0.01)	− 0.03 (0.03)	− 0.16 (0.04)
	Phantom/field	0.42	0.44	0.63	0.85	0.67
Absolute mean	Difference	0.04 (0.00)	0.04 (0.00)	0.06 (0.01)	0.08 (0.02)	0.16 (0.04)

Values represent the proportion of transects within each gap class. Standard errors are shown in parentheses

($n = 7$), we compared fractional cover agreement between Phantom and Sequoia multi-spectral imagery. Due to the relatively small sample sizes, we did not separate analysis by ecological site which is typically done for I & M data interpretation (see Karl and Herrick 2010).

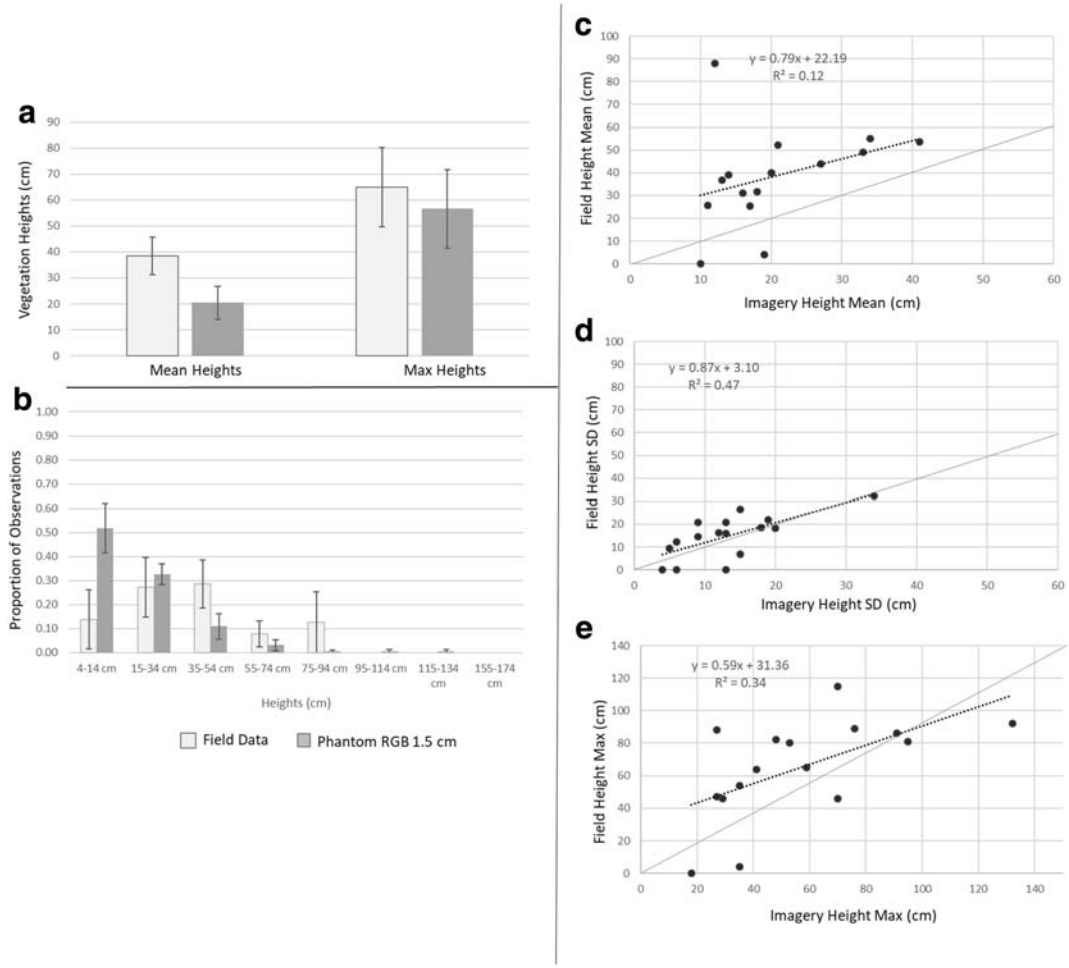

Fig. 9 Agreement between field and imagery methods of estimating vegetation heights. **a** Bar graphs show mean and maximum vegetation heights across all plots with 95% confidence intervals ($n = 16$). **b** Histogram showing proportion of values within height bins with 95% confidence intervals. **c** Scatterplot and linear regression for mean height. **d** Scatterplot and linear regression for height standard deviation. **e** Scatterplot and linear regression (dotted lines) for maximum vegetation heights. Solid lines represent 1:1 agreement

Results

Method agreement—fractional cover

The woody vegetation cover class showed the strongest linear relationship between field and image measurements ($R^2 = 0.82$; Fig. 6), followed by annual herb/grass ($R^2 = 0.79$), bare-ground ($R^2 = 0.69$), and perennial herb/grass ($R^2 = 0.24$). Mean fractional cover across all plots was similar between field and imagery estimates for each of the four classes (Table 2). Mean method differences ranged from as small as −0.009 (perennial herb) to as large as −0.062 (bare-ground). Bare-ground had the largest absolute mean difference (0.145), followed closely by annual herb/grass (0.134). Perennial herb/grass and woody had absolute mean differences of 0.052 and 0.047, respectively. Indicator value variation between plots was higher (i.e., larger standard errors) for imagery compared with field methods for each of the cover classes.

Fractional cover sensor comparison

We found minimal differences in linear relationships between the Phantom RGB camera and Sequoia multispectral sensor in terms of fractional cover agreement with field measurements (Fig. 7). Similarly, average fractional cover and cover differences with field methods were < 3% different for each cover class (Table 3).

Method agreement—canopy gaps

Proportion of inter-canopy gaps were generally underestimated for each size class (Fig. 8a; Table 4). The greatest relative underestimations (proportional to the mean value) occurred at small gaps sizes (e.g., 25–50 cm) and steadily shrank as gap sizes increased. Variance (illustrated with confidence intervals) between field and imagery estimates was very similar. Linear relationships between field and imagery improved as the size of the gaps increased (Fig. 8b).

Method agreement—vegetation heights

Imagery methods underestimated mean vegetation heights by 18 cm on average and underestimated maximum vegetation heights on average by 8 cm (Fig. 9a). Regarding the proportion of height observations within histogram bins, nearly 50% of imagery observations were within the 4–14 cm bin, while field methods had only 14% of observations within that range (Fig. 9b). Conversely, there was a much higher proportion of field observations within the height bins from 35 to 54 cm (29% v. 11%), 55–74 cm (8% v. 3%), and 75–94 cm (13% v. 0%). The linear relationship of mean heights was weak ($R^2 = 0.12$), mostly due to one plot with a dead woody plant that was too thin to be detected with imagery (Fig. 9c). Removing this one plot from analysis improved the linear relationship to $R^2 = 0.46$. Height standard deviation had $R^2 = 0.47$ (Fig. 9d) and maximum height had $R^2 = 0.34$ (Fig. 9e). Mean and maximum vegetation height were overpredicted (compared to field measures) at some plots because tall woody plants were not encountered with the field methods.

Discussion

Fractional cover

Because imagery and field methods of observing vegetation cover have inherent mechanical differences (i.e., pin drops v. classified pixels) and possible co-registration error, perfect agreement between indicator values is not expected. Image-based measures should be, however, strongly related to field measures to be considered a reliable tool worth adopting for rangeland monitoring. Though we found strong relationships between imagery and field estimates of fractional cover, some classes could be improved with small workflow adjustments detailed in the following two paragraphs.

It was difficult to find useable training samples for perennial herb/grass because there were so few of them to begin with and because potential samples were often too small and indistinguishable from adjacent pixels. This often led to omitting the class or poor results (e.g., under- or over-prediction). The imagery resolution was generally too coarse to identify and classify perennial bunchgrasses found in this study area. We would recommend imagery ≤ 1 cm GSD to identify individual bunchgrasses and other herbaceous plants as demonstrated in other projects (Cunliffe et al. 2016; Fraser et al. 2016; Gillan et al. 2019). Even at this fine resolution, however, separating herbaceous species from each other will be challenging (Gearhart et al. 2013; Laliberte et al. 2010b; Lu and He 2017).

Though the annual herb/grass and bare-ground classes had strong linear relationships with field methods, they had the highest mean absolute differences. The classifications often confused annual herb/grass (mostly cheatgrass) and bare-ground, a significant problem given the concern of cheatgrass expansion in the district. Confusion was primarily caused by cheatgrass that had senesced to a yellow/brown color making it difficult to separate from bare-ground. Separation may have been better in the spring while the cheatgrass was still green and easily distinguished from bare-ground. Imagery collected in the spring, however, may not capture other annuals such as prickly lettuce (*Lactuca serriola*) or perennials such as bottlebrush squirrel tail (*Elymus elymoides*).

Vegetation phenology is critical to identify species or functional groups within imagery, more so than identifying the same features with field methods (Hunt et al. 2003; Lass and Calihan 1997). As with any image classification, distinguishing features of interest is highly dependent on the spectral and spatial uniqueness of the classes (Laliberte and Rango 2011). Integrating drone imagery will require a re-thinking of when monitoring occurs to maximize feature detectability. Depending on the objectives of the inventory and monitoring, multiple acquisitions may be required in a year.

We found little difference in fractional cover agreement between the Phantom RGB camera and the Parrot Sequoia multi-spectral sensor. Other research has demonstrated the ability of RGB imagery to successfully classify cover (Cruzan et al. 2016; Laliberte et al. 2010a; Meng et al. 2018). In addition to lower cost, RGB sensors generally offer higher spatial resolution compared with multi-spectral sensors, an advantage for identifying small plants and generating detailed point clouds. In theory, multi-spectral sensors offer additional bandwidth from which to separate species based on spectral differences (Laliberte et al. 2011a), though we found no discernible advantage in this study. Additionally, multi-spectral sensors can also be radiometrically calibrated to reflectance values which could improve consistency of repeat image classifications and aid the development of spectral libraries. Other sensors including LiDAR and hyperspectral have been demonstrated on drones to characterize dryland vegetation cover and structure (Mitchell et al. 2012; Sankey et al. 2017). Their data may help to distinguish more cover classes than RGB and multi-spectral. However, the additional cost and technical challenges of these sensors may make them less desirable for mass adoption and reducing monitoring costs.

Canopy gaps

Similar to our findings, Karl et al. (2012) found that correlations between imagery and field estimates improved as the gap sizes increased, and gaps > 50 cm were reliably estimated from imagery in a variety of plant communities. In this research, consistent underestimation of canopy gaps at each size class had two main causes. The first was misclassifying bare-ground as annual herb/grass. The second (and less frequent) cause was scale (specifically grain) differences between field and imagery observations. The imagery, and subsequent grouping of pixels into objects, could not see small diameter branches or sparse vegetation the field observer could see. Take, for example, a group of shrubs close to each other. The imagery classification may perceive no gaps between the shrubs, while the field observer may observe that there are in fact gaps of at least 25 cm between the branch canopies.

Canopy gaps are an example of an indicator that has the potential to be improved instead of simply replicated by drone imagery. Field-based measures of canopy gaps are a 1-dimensional representation of erosional force connectivity that is typically integrated over multiple directions in the plot to provide a composite value (Webb et al. 2014). Drone imagery could open up more meaningful 2-D or 3-D measurements of the same phenomenon. For example, with drone-based classifications, the size and configuration of bare ground patches parallel to the slope (indicator of water erosion potential) could be separated from the effects of bare ground patches in line with prevailing winds (indicator of wind erosion potential). Similarly, Ludwig et al. (2007) used two-dimensional information on bare ground distribution to create an index related to a site's ability to retain resources (i.e., a "leakiness" index).

Vegetation heights

The differences between imagery and field estimates of woody vegetation heights were caused primarily by the mechanics of each method, and additionally by imperfect referencing (i.e., scale-bar). For mean height, the field method averaged 30 measurements of the tallest

part of the plant that was encountered within a 15-cm radius of a rod placement. Most of these observations were high up on the plant. The point cloud/CHM methods observed all aspects of the plant, from the crown to the base. Naturally, numerous observations on the lower part of the plant brought down the average. The maximum vegetation height in a plot was generally underestimated by the imagery due to poorly modeling plant extremities that were too fine or small to detect. This is a well-known trait of photogrammetric reconstruction methods (Cunliffe et al. 2016; Gillan et al. 2014; Olsoy et al. 2018), but is not necessarily a limitation in a rangeland monitoring context. Maximum vegetation height is a convenient indicator to measure in the field, but it may not hold any specific ecological value. Drone-based photogrammetric point clouds can provide thousands of measurements, enabling a more detailed and synoptic look at vegetation heights, including the ability to quantify observations per height bin, analyze height variance, and calculate vegetation volume. This technique will improve our ability to estimate biomass and carbon storage (Cunliffe et al. 2016), parameterize surface roughness for wind erosion modeling (Webb et al. 2014), quantify fuels for prescribed or uncontrolled fires (Leis and Morrison 2011), and assess the quality of wildlife habitat (Olsoy et al. 2018). In NCD, for example, greater sage-grouse habitat could be assessed with drone-based vegetation structure data, including the height, cover, and shape of sagebrush (Stiver et al. 2015).

Developing best practices

The workflow presented in the paper is just one of many possible paths to estimate these indicator values, and further work is needed to validate UAS-based techniques for estimating I & M indicators in different rangeland systems. Additionally, the choices of hardware, software, image acquisition, and processing specifications are large and growing. Identifying drone-imagery best practices could be accelerated with an online workflow repository. Given the high interest in this technology, a website like this could spur collaboration and advancement in ways that published literature alone cannot. A few existing protocol repositories include Protocols Exchange (https://www.nature.com/protocolexchange) and Protocols.IO (http://protocols.io). Cunliffe and Anderson (2019), for example, published a protocol to collect drone imagery for biomass estimation in Protocols Exchange (https://doi.org/10.1038/protex.2018.134). Alternatively, it could be advantageous to share workflows through a website dedicated to rangeland I & M (e.g., the Landscape Toolbox, www.landscapetoolbox.com), where drone-based monitoring could be embedded within the larger context of rangeland data collection theory and field protocols.

Is drone monitoring worth the effort?

In large monitoring programs like AIM that collect a diverse suite of data, drones will not replace most of the field methods. Even from very high-resolution imagery, it can be challenging to identify fine-scale features (e.g., grass and forb species identification, biological crusts) and carry out qualitative assessments of land health (i.e., in situ multi-factor interpretations of ecosystem condition or trend). However, drone-imagery methods could be used in a more supplemental capacity in which the modes of integration can be customized to the specific management needs of the locality. In the NCD, for example, drone imagery could be collected to improve estimates of bare-ground or cheatgrass cover in a post-fire rehabilitation area. This could take the form of expanding the size of existing monitoring plots, or collecting imagery at new plots without field measures.

Drone-imagery-based indicators will complement other remote sensing efforts that "upscale" field data to satellite imagery products (see Jones et al. 2018; McCord et al. 2017; Xian et al. 2015). The upscaled products have the advantage of covering entire field offices but the indicators are limited to fractional cover of a few general classes (bare-ground, woody, perennial herb, etc). Drone imagery can observe features that cannot be modeled to satellite imagery, such as canopy gaps, vegetation heights, and identification of some vegetation species.

Conclusion

Due to their low cost, ability to image dozens of hectares per flight, and extreme portability, small UAS are likely to become a standard tool for rangeland inventory and monitoring. They will be integrated with existing field efforts in order to observe larger and more representative portions of the landscape and to measure indicators not

easily measured on the ground. We demonstrated a workflow to estimate three rangeland vegetation indicators, reported agreement with their counterpart field method, and provided recommendations for workflow improvements. These methods could serve as a starting point for other drone-based I & M efforts in sagebrush steppe ecosystems. Despite the success of this and other research demonstrations, we face a challenge in developing a suite of monitoring methods that are useful for supporting management decisions (e.g., accurate, repeatable, and cost-effective) across varied rangeland systems. The time is right to develop an online space that facilitates the co-creation of repeatable workflows and curates best practices for a variety of rangeland indicators.

Acknowledgments We thank Andrew Johnson, geographer at Eagle Lake Field Office, for help coordinating this research with field crews. We also thank Eric Panebaker, aviation manager of BLM Northern California District, for permitting drone flights.

Funding information Travel and data collection were funded by USDA ARS Jornada Experimental Range.

Compliance with ethical standards

Conflict of interest The authors declare that they have no conflict of interest.

References

Allen, C. R., Angeler, D. G., Fontaine, J. J., Garmestani, A. S., Hart, N. M., Pope, K. L., & Twidwell, D. (2017). Adaptive management of rangeland systems. In *Rangeland Systems: Processes, management and challenges* (pp. 373–394).

Baena, S., Moat, J., Whaley, O., & Boyd, D. S. (2017). Identifying species from the air: UAVs and the very high resolution challenge for plant conservation. *PLoS One, 12*(11), e0188714. https://doi.org/10.1371/journal.pone.0188714.

Booth, D. T., & Cox, S. E. (2008). Image-based monitoring to measure ecological change in rangeland. *Frontiers in Ecology and the Environment, 6*(4), 185–190. https://doi.org/10.1890/070095.

Booth, D. T., & Cox, S. E. (2009). Dual-camera, high-resolution aerial assessment of pipeline revegetation. *Environmental Monitoring and Assessment, 158*, 23–33. https://doi.org/10.1007/s10661-008-0562-5.

Booth, D., & Cox, S. (2011). Art to science: tools for greater objectivity in resource monitoring. *Rangelands, 33*(4), 27–34. https://doi.org/10.2111/1551-501x-33.4.27.

Breckenridge, R. P., Dakins, M., Bunting, S., Harbour, J. L., & White, S. (2011). Comparison of unmanned aerial vehicle platforms for assessing vegetation cover in sagebrush steppe ecosystems. *Rangeland Ecology & Management, 64*(5), 521–532. https://doi.org/10.2111/REM-D-10-00030.1.

Burnett, C., & Blaschke, T. (2003). A multi-scale segmentation/object relationship modelling methodology for landscape analysis. *Ecological Modelling, 168*(3), 233–249. https://doi.org/10.1016/S0304-3800(03)00139-X.

Carbonneau, P. E., & Dietrich, J. T. (2016). Cost-effective non-metric photogrammetry from consumer-grade sUAS: implications for direct georeferencing of structure from motion photogrammetry. *Earth Surface Processes and Landforms, 42*(3), 473–486. https://doi.org/10.1002/esp.4012.

Cruzan, M. B., Weinstein, B. G., Grasty, M. R., Kohrn, B. F., Hendrickson, E. C., Arredondo, T. M., & Thompson, P. G. (2016). Small unmanned aerial vehicles (micro-UAVs, drones) in plant ecology. *Applications in Plant Sciences, 4*(9), 1600041. https://doi.org/10.3732/apps.1600041.

Cunliffe, A., & Anderson, K. (2019. Measuring above-ground biomass with drone photogrammetry: data collection protocol. *Protocol Exchange*. https://doi.org/10.1038/protex.2018.134.

Cunliffe, A. M., Brazier, R. E., & Anderson, K. (2016). Ultra-fine grain landscape-scale quantification of dryland vegetation structure with drone-acquired structure-from-motion photogrammetry. *Remote Sensing of Environment, 183*, 129–143. https://doi.org/10.1016/j.rse.2016.05.019.

Duniway, M. C., Karl, J. W., Schrader, S., Baquera, N., & Herrick, J. E. (2012). Rangeland and pasture monitoring: an approach to interpretation of high-resolution imagery focused on observer calibration for repeatability. *Environmental Monitoring and Assessment, 184*(6), 3789–3804. https://doi.org/10.1007/s10661-011-2224-2.

Eltner, A., Kaiser, A., Castillo, C., Rock, G., Neugirg, F., & Abellan, A. (2015). Image-based surface reconstruction in geomorphometry – merits, limits and developments of a promising tool for geoscientists. *Earth Surface Dynamics Discussions, 3*(4), 1445–1508. https://doi.org/10.5194/esurfd-3-1445-2015.

Fraser, R. H., Olthof, I., Lantz, T. C., & Schmitt, C. (2016). UAV photogrammetry for mapping vegetation in the Low-Arctic. *Arctic Science, 102*(June), 1–51. https://doi.org/10.1139/as-2016-0008.

Gearhart, A., Booth, D. T., Sedivec, K., & Schauer, C. (2013). Use of Kendall's coefficient of concordance to assess agreement among observers of very high resolution imagery. *Geocarto International, 28*(6), 517–526. https://doi.org/10.1080/10106049.2012.725775.

Gillan, J. K., Karl, J. W., Duniway, M., & Elaksher, A. (2014). Modeling vegetation heights from high resolution stereo aerial photography: an application for broad-scale rangeland monitoring. *Journal of Environmental Management, 144*, 226–235. https://doi.org/10.1016/j.jenvman.2014.05.028.

Gillan, J., Karl, J., Elaksher, A., & Duniway, M. (2017). Fine-resolution repeat topographic surveying of dryland landscapes using UAS-based structure-from-motion photogrammetry: assessing accuracy and precision against traditional ground-based erosion measurements. *Remote Sensing, 9*(5), 437. https://doi.org/10.3390/rs9050437.

Gillan, J. K., McClaran, M. P., Swetnam, T. L., & Heilman, P. (2019). Estimating forage utilization with drone-based photogrammetric point clouds. *Rangeland Ecology & Management, 72*(4), 575–585. https://doi.org/10.1016/j.rama.2019.02.009.

Hardin, P., Jackson, M., Anderson, V., & Johnson, R. (2007). Detecting Squarrose knapweed (Centaurea virgata lam. Ssp. squarrosa Gugl.) using a remotely piloted vehicle: a Utah case study. *GIScience & Remote Sensing, 44*(3), 203–219. https://doi.org/10.2747/1548-1603.44.3.203.

Herrick, J. E., Zee, J. W. Van, McCord, S. E., Courtright, E. M., Karl, J. W., & Burkett, L. M. (2017). Monitoring manual for grassland, shrubland, and savanna ecosystems 2nd edn. Vol 1: Core Methods.

Hunt, E. R., Everitt, J. H., Ritchie, J. C., Moran, M. S., Booth, D. T., Anderson, G. L., et al. (2003). Applications and research using remote sensing for rangeland management. *Photogrammetric Engineering & Remote Sensing, 69*(6), 675–693. https://doi.org/10.14358/PERS.69.6.675.

James, M. R., & Robson, S. (2014). Mitigating systematic error in topographic models derived from UAV and ground-based image networks. *Earth Surface Processes and Landforms, 39*(10), 1413–1420. https://doi.org/10.1002/esp.3609.

James, M. R., Robson, S., D'Oleire-Oltmanns, S., & Niethammer, U. (2017). Optimising UAV topographic surveys processed with structure-from-motion: ground control quality, quantity and bundle adjustment. *Geomorphology, 280*, 51–66. https://doi.org/10.1016/j.geomorph.2016.11.021.

Jensen, J. L. R., & Mathews, A. J. (2016). Assessment of image-based point cloud products to generate a bare earth surface and estimate canopy heights in a woodland ecosystem. *Remote Sensing, 8*(50). https://doi.org/10.3390/rs8010050.

Jones, M. O., Allred, B. W., Naugle, D. E., & Mestas, J. D. (2018). Innovation in rangeland monitoring : annual, 30 m, plant functional type percent cover maps for U. S. rangelands, 1984–2017, 9(September). https://doi.org/10.1002/ecs2.2430.

Karl, J. W., & Herrick, J. E. (2010). Monitoring and assessment based on ecological sites. *Rangelands, 32*(6), 60–64. https://doi.org/10.2111/RANGELANDS-D-10-00082.1.

Karl, J. W., Duniway, M. C., & Schrader, T. S. (2012). A technique for estimating rangeland canopy-gap size distributions from high-resolution digital imagery. *Rangeland Ecology & Management, 65*(2), 196–207. https://doi.org/10.2111/REM-D-11-00006.1.

Karl, J. W., Gillan, J. K., Barger, N. N., Herrick, J. E., & Duniway, M. C. (2014). Interpretation of high-resolution imagery for detecting vegetation cover composition change after fuels reduction treatments in woodlands. *Ecological Indicators, 45*, 570–578. https://doi.org/10.1016/j.ecolind.2014.05.017.

Kendall, W. L., & Moore, C. T. (2012). Maximizing the utility of monitoring to the adaptive management of natural resources. In R. A. Gitzen, J. J. Milspaugh, A. B. Cooper, & D. S. Licht (Eds.), *Design and analysis of long-term ecological monitoring studies*. Cambridge: University of Cambridge Press.

Kuhn, M., & Quinlan, R. (2017). C5.0 decision trees and rule-based models. R package version 0.1.1.

Laliberte, A. S., & Rango, A. (2011). Image processing and classification procedures for analysis of sub-decimeter imagery acquired with an unmanned aircraft over arid rangelands. *GIScience & Remote Sensing, 48*(1), 4–23. https://doi.org/10.2747/1548-1603.48.1.4.

Laliberte, A. S., Browning, D. M., Herrick, J. E., & Gronemeyer, P. (2010a). Hierarchical object-based classification of ultra-high-resolution digital mapping camera (DMC) imagery for rangeland mapping and assessment. *Journal of Spatial Science, 55*(1), 101–115. https://doi.org/10.1080/14498596.2010.487853.

Laliberte, A. S., Herrick, J. E., Rango, A., & Winters, C. (2010b). Acquisition, orthorectification, and object-based classification of unmanned aerial vehicle (UAV) imagery for rangeland monitoring. *Photogrammetric Engineering & Remote Sensing, 76*(6), 661–672. https://doi.org/10.14358/PERS.76.6.661.

Laliberte, A. S., Goforth, M. a., Steele, C. M., & Rango, A. (2011a). Multispectral remote sensing from unmanned aircraft: image processing workflows and applications for rangeland environments. *Remote Sensing, 3*(12), 2529–2551. https://doi.org/10.3390/rs3112529.

Laliberte, A. S., Winters, C., & Rango, A. (2011b). UAS remote sensing missions for rangeland applications. *Geocarto International, 26*(2), 141–156. https://doi.org/10.1080/10106049.2010.534557.

Lass, L. W., & Calihan, R. H. (1997). Effects of phenological stage on detectability of yellow hawkweed (Hieracium pratense) and oxeye daisy (Chrysanthemum leucanthemum) with remote multispectral digital imagery. *Weed Technology, 11*, 248–256.

Leis, S. a., & Morrison, L. W. (2011). Field test of digital photography biomass estimation technique in tallgrass prairie. *Rangeland Ecology & Management, 64*(1), 99–103. https://doi.org/10.2111/REM-D-09-00180.1.

Louhaichi, M., Borman, M. M., & Johnson, D. E. (2001). Spatially located platform and aerial photography for documentation of grazing impacts on wheat. *Geocarto International, 16*(1), 65–70. https://doi.org/10.1080/10106040108542184.

Lu, B., & He, Y. (2017). Species classification using unmanned aerial vehicle (UAV)-acquired high spatial resolution imagery in a heterogeneous grassland. *ISPRS Journal of Photogrammetry and Remote Sensing, 128*, 73–85. https://doi.org/10.1016/j.isprsjprs.2017.03.011.

Ludwig, J. A., Bastin, G. N., Chewings, V. H., Eager, R. W., & Liedloff, A. C. (2007). Leakiness: a new index for monitoring the health of arid and semiarid landscapes using remotely sensed vegetation cover and elevation data. *Ecological Indicators, 7*(2), 442–454. https://doi.org/10.1016/j.ecolind.2006.05.001.

MacKinnon, W. C., Karl, J. W., Toevs, G. R., Taylor, J. J., Karl, M., Spurrier, C. S., & Herrick, J. E. (2011). BLM core terrestrial indicators and methods. Tech Note 440. Denver: US Department of the Interior, Bureau of Land Management, National Operations Center.

McCord, S. E., Buenemann, M., Karl, J. W., Browning, D. M., & Hadley, B. C. (2017). Integrating remotely sensed imagery and existing multiscale field data to derive rangeland indicators: application of Bayesian additive regression trees. *Rangeland Ecology & Management*, 1–12. https://doi.org/10.1016/j.rama.2017.02.004.

McGwire, K. C., Weltz, M. A., Finzel, J. A., Morris, C. E., Fenstermaker, L. F., & McGraw, D. S. (2013). Multiscale assessment of green leaf cover in a semi-arid rangeland with a

small unmanned aerial vehicle. *International Journal of Remote Sensing, 34*(5), 1615–1632. https://doi.org/10.1080/01431161.2012.723836.

Meng, B., Gao, J., Liang, T., Cui, X., Ge, J., Yin, J., et al. (2018). Modeling of alpine grassland cover based on unmanned aerial vehicle technology and multi-factor methods: a case study in the east of Tibetan Plateau, China. *Remote Sensing, 10*(2), 320. https://doi.org/10.3390/rs10020320.

Mitchell, J. E. (2010). *Criteria and indicators of sustainable rangeland management*. University of Wyoming Cooperative Extension Publication No. SM-56.

Mitchell, J. J., Glenn, N. F., Anderson, M. O., Hruska, R. C., & Charlie, A. H. (2012). Unmanned aerial vehicle ({UAV}) hyperspectral remote sensing for dryland vegetation monitoring hyperspectral image and signal sensing. *Idaho National Laboratory Preprint.*

Moffet, C. a. (2009). Agreement between measurements of shrub cover using ground-based methods and very large scale aerial imagery. *Rangeland Ecology & Management, 62*(3), 268–277. https://doi.org/10.2111/08-244R.1.

Montealegre, A. L., Lamelas, M. T., & De La Riva, J. (2015). A comparison of open - source LiDAR filtering algorithms in a mediterranean forest environment. *IEEE Journal of Selected Topics in Applied Earth Observations and Remote Sensing, 8*(8), 4072–4085. https://doi.org/10.1109/JSTARS.2015.2436974.

Navulur, K. (2007). *Multi-spectral image analysis using the object-oriented paradigm*. Boca Raton: CRC Press, Taylor and Francis Group.

Olsoy, P. J., Shipley, L. A., Rachlow, J. L., Forbey, J. S., Glenn, N. F., Burgess, M. A., & Thornton, D. H. (2018). Unmanned aerial systems measure structural habitat features for wildlife across multiple scales. *Methods in Ecology and Evolution, 9*(3), 594–604. https://doi.org/10.1111/2041-210X.12919.

Rango, A., Laliberte, A., Herrick, J. E., Winters, C., Havstad, K., Steel, C., & Browning, D. (2009). Unmanned aerial vehicle-based remote sensing for rangeland assessment, monitoring, and management. *Journal of Applied Remote Sensing, 3*(1), 033542. https://doi.org/10.1117/1.3216822.

Sankey, T. T., McVay, J., Swetnam, T. L., McClaran, M. P., Heilman, P., & Nichols, M. (2017). UAV hyperspectral and lidar data and their fusion for arid and semi-arid land vegetation monitoring. *Remote Sensing in Ecology and Conservation*, 1–14. https://doi.org/10.1002/RSE2.44.

Seefeldt, S. S., & Booth, D. T. (2006). Measuring plant cover in sagebrush steppe rangelands: a comparison of methods. *Environmental Management, 37*(5), 703–711. https://doi.org/10.1007/s00267-005-0016-6.

Smith, M. W., Carrivick, J. L., & Quincey, D. J. (2015). Structure from motion photogrammetry in physical geography. *Progress in Physical Geography, 40*(2), 247–275. https://doi.org/10.1177/0309133315615805.

Snavely, N., Seitz, S. M., & Szeliski, R. (2008). Modeling the world from Internet photo collections. *International Journal of Computer Vision, 80*(2), 189–210. https://doi.org/10.1007/s11263-007-0107-3.

Stiver, S. J., Thomas Rinkes, E., & Naugle, D. E. (2015). Sage-grouse habitat assessment framework: a multiscale assessment tool. *Technical reference 6710–1.* Denver, CO.

Swetnam, T. L., Gillan, J. K., Sankey, T. T., McClaran, M. P., Nichols, M. H., Heilman, P., & McVay, J. (2018). Considerations for achieving cross-platform point cloud data fusion across different dryland ecosystem structural states. *Frontiers in Plant Science, 8*(January), 2144. https://doi.org/10.3389/fpls.2017.02144.

Taylor, J., Kachergis, E., Toevs, G., Karl, J., Bobo, M., Karl, M, Miller, S., & Spurrier, C. (2014). AIM-monitoring: a component of the BLM assessment, inventory, and monitoring strategy. Tech Note 445. Denver: US Department of the Interior, Bureau of Land Management, National Operations Center.

Toevs, G. R., Karl, J. W., Taylor, J. J., Spurrier, C. S., Karl, M. S., Bobo, M. R., & Herrick, J. E. (2011). Consistent indicators and methods and a scalable sample design to meet assessment, inventory, and monitoring information needs across scales. *Rangelands, 33*(4), 14–20. https://doi.org/10.2111/1551-501X-33.4.14.

US Bureau of Land Management. (2007). Eagle Lake field office resource management plan and environmental impact statement. Susanville, CA.

Vautherin, J. (2016). Photogrammetric accuracy and modeling of rolling shutter cameras. *EuroCOW 2016, the European Calibration and Orientation Workshop (Presentation), 10–12* February 2016, Lausanne, Switzerland. https://doi.org/10.5194/isprsannals-III-3-139-2016.

Webb, N. P., Herrick, J. E., & Duniway, M. C. (2014). Ecological site-based assessments of wind and water erosion : informing accelerated soil erosion management in rangelands. *Ecological Applications, 24*(6), 1405–1420. https://doi.org/10.1890/13-1175.1.

Westoby, M. J., Brasington, J., Glasser, N. F., Hambrey, M. J., & Reynolds, J. M. (2012). 'Structure-from-motion' photogrammetry: a low-cost, effective tool for geoscience applications. *Geomorphology, 179*, 300–314. https://doi.org/10.1016/j.geomorph.2012.08.021.

Xian, G., Homer, C., Rigge, M., Shi, H., & Meyer, D. (2015). Characterization of shrubland ecosystem components as continuous fields in the northwest United States. *Remote Sensing of Environment, 168*, 286–300. https://doi.org/10.1016/j.rse.2015.07.014.